École Polytechnique

Master REST

PV in Industry

Advanced Characterization

Authors:
David Mota
Ismail Kaaya
Leonhard Probst

Supervisor:
Raphaël Lachaume

March 16, 2016

ÉCOLE
POLYTECHNIQUE
UNIVERSITÉ PARIS-SACLAY

Abstract

The objective is to study the effect of different experimental parameters on the reconstruction of the density of states (DoS) and to verify the viability of the 1D/2D simulation model developed at GeePs. Beside the calculation of the DoS through the modulated photo-current method (MPC), the ambipolar minority carrier diffusion length is measured through steady state photocarrier grating (SSPG) and the majority carrier lifetime / mobility product is measured through steady state photo-conductivity (SSPC). The measurements were observed to be in agreement with the theoretical simulations, but further experiments are needed to accurately conclude the need of a 2D simulation for the MPC experiment.

Contents

1 Introduction

In this report we study the transport parameters of a-Si:H thin films. The electronic measurement techniques which can be used are classified into two main categories, depending on the type of samples they are concerned with.

The samples can either be in a sandwich configuration (Fig. 1a) with a front rectifying contact (e.g. Schottky) and a back contact (which can also be the substrate if it is conductive). For this configuration, the current flows perpendicular to the surface.

Otherwise the samples can be in a coplanar configuration (Fig. 1b), where the current flows parallel to the surface. Two electrode pairs with different gaps (d) can be used to eliminate the contact resistances. In the laboratory, two different coplanar samples (A and B) with only one electrode pair were investigated. Sample A is marked as "PW51109A" and sample B as "PW51110A" in the numbering system used in the laboratory. The contact resistances are considered to be negligible compared to the resistance of the thin-film between the two electrodes. The dimensions of the samples as shown in Fig. 1b were:

$$h = 2 \text{ cm},$$
$$d = 1 \text{ mm},$$
$$t_A = 0.5 \text{ μm}, \ t_B = 1.0 \text{ μm}.$$

Three planar characterization techniques were utilized, namely the steady state photocarrier grating (SSPG), the steady state photo-conductivity (SSPC) and the modulated photo-current (MPC). It is not the main aim of this report to describe in details these characterization techniques, however for the sake of introduction, each technique will be explained briefly in the next section.
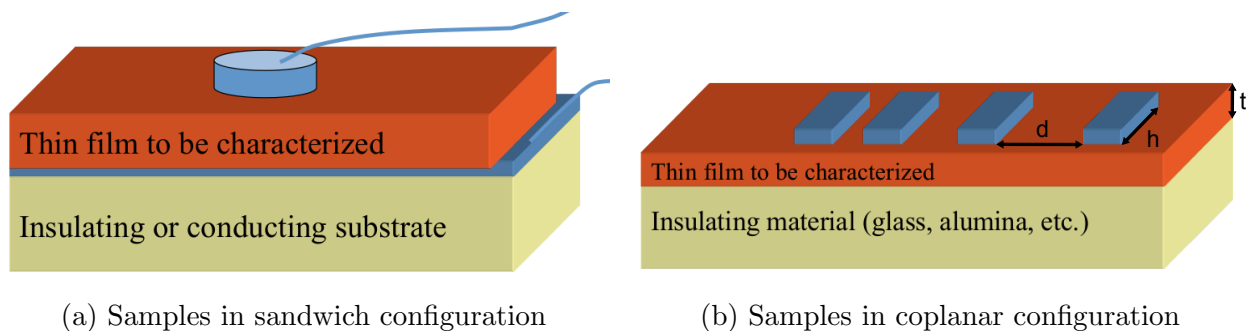

(a) Samples in sandwich configuration (b) Samples in coplanar configuration

Fig. 1: Different types of sample configurations

2 Measurement techniques in planar configuration

2.1 Steady-state photocarrier grating

2.1.1 Overview of SSPG

The steady-state photocarrier grating technique allows the determination of the ambipolar diffusion length in low-mobility semiconductors and provides access to the minority-carrier properties in terms of the mobility lifetime product. The SSPG technique is based on the carrier diffusion under the presence of a spatial sinusoidal modulation in the photogeneration rate achieved by the interference of two coherent laser beams – technically achieved by splitting the beam from a laser by a beam splitter. The resulting modulation in the photogeneration rate in the semiconductor bulk induces a so-called photocarrier grating with a spatial modulation in the excess carrier densities. From photocurrent measurements at different grating periods the ambipolar diffusion length can be determined. Figure 2 illustrates the beams L_1 and L_2 which represent plane waves with wavelength λ which impinge on the semiconductor.
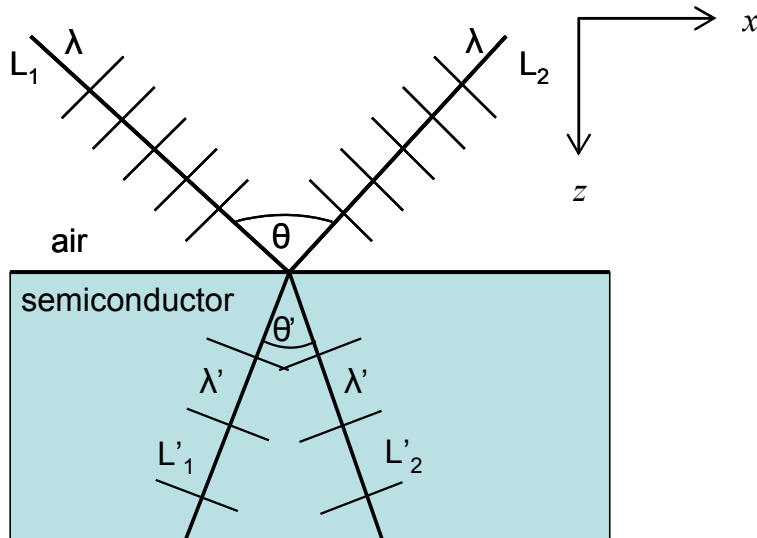

Fig. 2: Sketch of the interference experiment with two plane waves from the laser beams L_1 and L_2. [2]

In the SSPG experiments, one measures the ratio β by exploiting two conditions of the laser-beam arrangement at a given Λ:

$$\Lambda = \frac{\lambda}{[2sin(\frac{\theta}{2})]} \tag{1}$$

where λ is the laser wavelength and θ the angle between the two beams (note it is the only parameter that enters the equation). The Ritter, Zeldov and Weiser 'RZW' (1986) analysis suggests to exploit two conditions of the laser-beam arrangement (Fig. 2), one measurement under coherent conditions, current with interference I_{wi} and one measurement under incoherent conditions, current without interference I_{woi} between the electrodes of the sample. Were I_{wi} and I_{woi} are lock-in amplifier

measurements under coherent and incoherent conditions.

$$\beta(\Lambda) = \frac{I_{wi}}{I_{wo}} \tag{2}$$

The parameter $\beta(\Lambda)$ is related with the ambipolar diffusion length L_d according to:

$$\beta(\Lambda) = 1 - \frac{2\phi}{[1 + (2\pi L_d/\Lambda)^2]^2} \tag{3}$$

From a measured set of β values at a number of Λ positions, a fit can be made with the two fit parameters L_d and ϕ. While L_d is the diffusion length that one wants to determine, ϕ is a fit parameter, typically between 0.5 and 1, which contains information on the grating quality, the intensity dependence of the photoconductivity and the ratio between dark and total current under illumination [6]. Equation 3 can be changed to the form

$$(1 - \beta)^{-1/2} = [(2\phi)^{-1}2(1/L_d)^2](2\pi/\Lambda)^2 + (2\phi)^{-1/2} \tag{4}$$

in which measured β values are processed to be ordinate values. Here L_d and ϕ are determined from linear fits (the so called Balberg fits/plots).

2.1.2 Experimental set-up

A variety of experimental set-ups are possible for the SSPG technique. A common feature is the splitting of a laser beam which is then guided symmetrically onto the sample in order to induce an interference grating. In our experiment we used the SSPG set-up as in Fig. 3. The laser beam was divided into two beams by a separator cube, one beam is AC since it is modulated by a chopper and the second beam (perpendicular) will be DC and is reflected onto the sample by the cylindrical plane mirror MC7. The AC beam is reflected onto the central flexible mirror MCA which is then reflected onto each of the fixed mirrors MF1-MF9 before the beam is reflected onto the sample at angle θ from the DC beam.The angle θ determines the period of grating Λ of interference induced by superposition of the Laser beams on the sample surface (i.e when the polarization of the light of the two beams is vertical). In opposite case when the polarization is horizontal, interference will not occur. The program then traces the parameter equation 3 and fits the curve of β and Λ from which it computes the value of the diffusion length L_d.

2.2 Steady State Photo-Conductivity

The SSPC measurement is largely used to study trapping and recombination in semiconductors and to extract parameters connected to the defects of a material. The photo-current through a coplanar polarized sample with the voltage is measured in steady state while the probe is illuminated by photons with an energy higher than the band gap of the probe. This measurement is done for different temperatures as well as different photon intensities, which allows to derive the photo-conductivity and the majority carrier mobility-lifetime product $\mu_n \tau_n$.
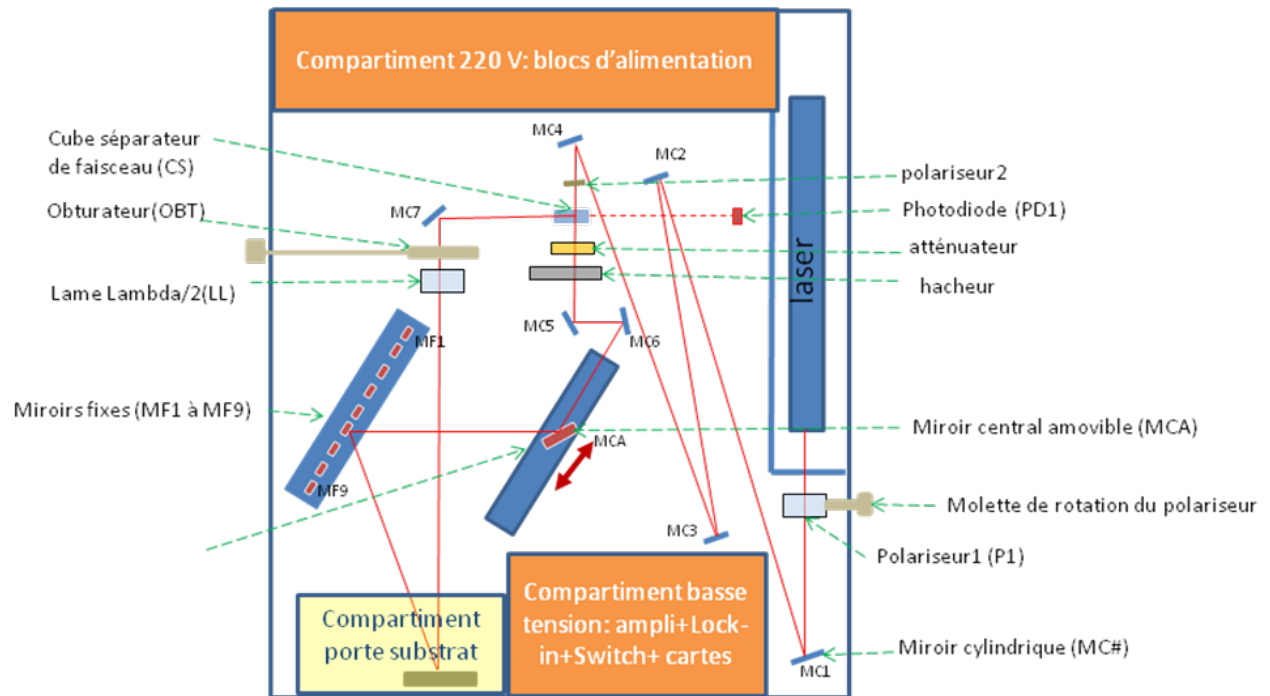
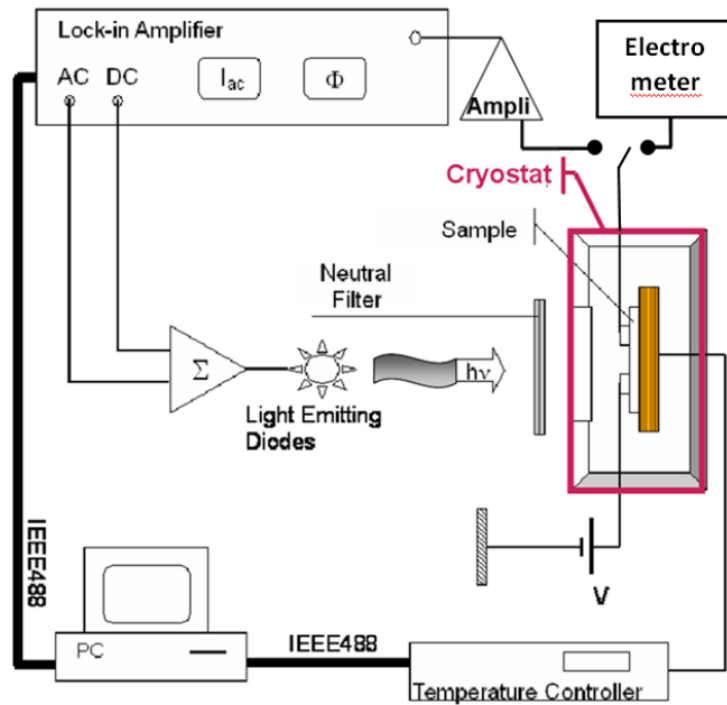Fig. 3: Diagram showing optical components and laser beam path. [4]

Fig. 4: Basic measurement system for SSPC (electrometer) and MPC (Lock-in Amplifier). [1]

2.2.1 Laboratory setup

Fig. 4 shows a basic laboratory setup for SSPC. The temperature of the probe is controlled with a cryostat. A voltage is applied to the probe and the current is measured with an electrometer under illumination produced with LEDs. A neutral filter can be used to further reduce the intensity of the light. The intensity of the LEDs could also be modulated and the current be measured with a lock-in amplifier (this will be covered in section 2.3).

2.2.2 Mathematical modeling

If the sample is kept at a certain temperature T and if an electric field E as well as a monochromatic photon flux F_{dc} is applied onto the sample of thickness h, the photo-current I_{ph} which can be measured in an infinitesimal thin layer dx of the sample is:

$$dI_{ph}(x) = hE\sigma_{ph}(x)dx \tag{5}$$

Where x is the depth in the layer and σ_{ph} is the photo-conductivity described in (6).

$$\sigma_{ph}(x) = q(\mu_n \Delta n(x) + \mu_p \Delta p(x)) \tag{6}$$

Where Δn and Δp are the excess carrier densities generated under illumination.

In a-Si:H, the transport is dominated by electrons (n-type material in nature) which means that the mobility lifetime product for electrons is much higher than that for holes ($\mu_n \tau_n \gg \mu_p \tau_p$). This fact can be used to simplify the equation for the photo-conductivity under a particular photon flux F_{dc}, which is defined in (7).

$$\sigma_{ph}(x) = q\mu_n \Delta n(x) = q\mu_n \tau_n G(x) = q\mu_n \tau_n (1 - R)F_{dc}\eta\alpha \exp(-\alpha x) \tag{7}$$

Where R is the reflection coefficient, η is the quantum efficiency and α is the absorption coefficient of the material.

If we solve the integral of (5) between 0 and the thickness of the material d while using (7) for σ_{ph}, we can obtain:

$$I_{ph} = I - I_{obs} = hEq\mu_n \tau_n (1 - R)F_{dc}\eta\alpha \int_0^d \exp(-\alpha x)dx \tag{8}$$

Where τ_n is taken as constant throughout x, which might not be true in reality as the light absorption varies through x. This could influence both parameters, mobility μ_n as well as lifetime τ_n.

If the the photon energy is higher than the band gap, the quantum efficiency η is approximately 1. This leads us to the mobility lifetime product:

$$\mu_n \tau_n = \frac{I - I_{obs}}{hEq(1 - R)F_{dc}(1 - \exp(-\alpha d))} \tag{9}$$

2.3 Modulated Photo-Current (MPC)

The MPC technique is a method that allows to study the density of states (DoS) of intrinsic, amorphous and crystalline semiconductors. It uses the same setup described in the SSPC experiment. In this experiment the sample is illuminated with a light source that has a continuous intensity and a sinusoidal intensity with frequency ω. This source will consequently generate electron hole pairs with a steady state regime (G_{dc}) and AC regime (G_{ac}). The modulus of the AC photocurrent (I_{ac}) and its phase shift (ϕ) with the generation rate is then recorded and used to extract information about the DoS.
Depending on the AC frequency, different physical processes can become more relevant than others. To analyze the output data of the experiment, two different regimes are used, depending on the AC frequency: the high frequency regime (HF) and the low frequency regime (LF).

2.3.1 MPC-HF

The high frequency regime is dominated by quick carrier capture and emission from empty gap states to the conduction band. The following equation allows to obtain the quantity N(E):

$$\frac{N(E)c_n}{\mu_n} = \frac{2}{\pi k_B T} S q \xi G_{ac} \frac{\sin(\phi)}{|I_{ac}|} \tag{10}$$

Where ξ is the electric field between the electrodes, S the section area of the current flow, q the electron charge, k_B the Boltzmann constant, c_n the electron capture coefficient and μ_n the electron mobility.

If $\mu_n \tau_n >> \mu_p \tau_p$, it is possible to have the following expression for $E_{\omega n}$:

$$E_C - E_n = k_B T ln \left(\frac{\nu_n}{\omega} \right) \tag{11}$$

Where $\nu_n = c_n N_C$ is the electron attempt-to-escape frequency and N_C is the effective conduction band density of states.

2.3.2 MPC-LF

The low frequency regime which is also called the recombination regime is dominated by the recombination of carriers in partially-filled gap states located at E_{tn}. E_{tn} is generally located around the center of the effective band gap, thus only having relevance in the low frequency regime. It is important to note that in this case ϕ has small values because most of the captured carriers are not re-emitted. The LF DoS can be deduced from:

$$N(E_{tn}) = 2 \frac{G_{dc}}{k_B T} \frac{\tan(\phi)}{\omega} \tag{12}$$

and E_{tn} can be obtained from:

$$E_C - E_{tn} = k_B T ln \left(\frac{\mu_n N_C S q \xi}{|I_{dc}|} \right) \tag{13}$$
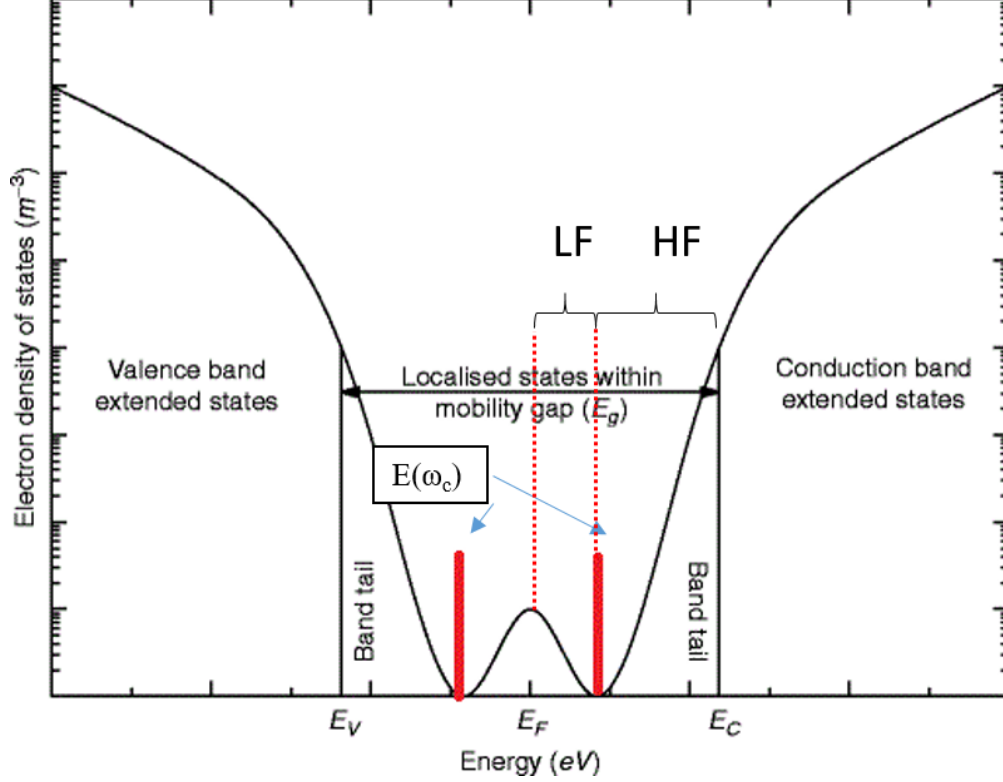

Fig. 5: Explanatory figure for MPC

Figure 5 shows in a pictorial representation of the high HF and LF regimes and cutoff frequency.

2.3.3 Cutoff frequency

Although the high frequency regime is valid for $\omega >> \bar{n}_{dc} + \bar{p}_{dc}$, with $\bar{n}_{dc} = n_{dc} C_n$ and $\bar{p}_{dc} = p_{dc} C_p$; and the low frequency is valid for $\omega << \bar{n}_{dc} + \bar{p}_{dc}$, in practice a cutoff frequency is defined $\omega_c = \bar{n}_{dc} + \bar{p}_{dc}$ over which the HF regime is valid and bellow which the LF regime is valid. Where p_{dc} and n_{dc} correspond respectively to the generated holes and electrons densities due to the DC light flux.

An easy way to estimate ω_c is by analyzing the linearity of $tan(\phi)$ as a function of frequency (ω). The data that is in the LF regime should respect equation 12, thus $tan(\phi)$ should be linear to ω. By this means the cutoff frequency can be estimated by analyzing the linearity of $tan(\phi)$ vs ω. This is shown in figure 6.

As it can be seen in the example of figure 6, the necessary linearity for the LF validity (displayed in the line) is never satisfied by the data (displayed by the dots), because in practice it is difficult to isolate the LF regime from the HF. For the LF reconstruction of the DoS the lowest frequency was used.
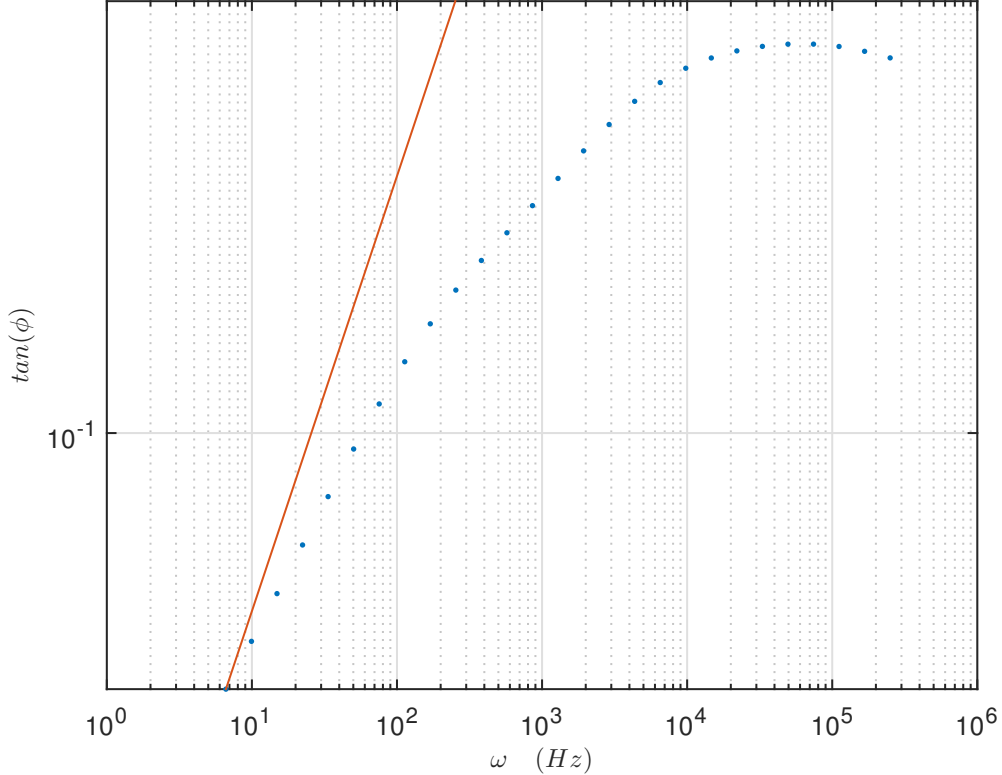
Fig. 6: Empirical estimation of the cutoff frequency for the sample 1 under red light illumination

3 Experimental Results and Discussion

Two samples of hydrogenated amorphous silicon thin films (a-Si:H) of different thicknesses (**sample A:** 0.5 µm) and (**sample B:** 1.0 µm) were studied using all the three experiments described in section 2 in order to characterize their transport properties. It is not the main purpose of our report to review the theoretical development and basic properties of a-Si:H which can be found in many literature, e.g. [3]. For the sake of simplicity and as a reminder for the reader, Table 1 shows the order of magnitude of the main transport parameters found for 'standard' a-Si:H.

Parameter	Order of magnitude	units
Activation Energy	0.6 - 0.8	eV
Extended states electron mobility	10 - 40	$cm^2V^{-1}s^{-1}$
Mobility lifetime product at 300K of electron	$5 \times 10^{-8} - 5 \times 10^{-6}$	cm^2V^{-1}
Mobility lifetime product at 300K of holes	$1 \times 10^{-9} - 1 \times 10^{-8}$	cm^2V^{-1}
Capture coefficient of conduction band tail states	10^{-8}	cm^3s^{-1}
Attempt to escape frequency	5×10^{11}	s^{-1}
Minority diffusion length at 300K	100 - 300	nm

Table 1: Order of magnitude of the main transport properties [3]

9

At first, the two samples shall be discussed separately according to the characterization technique used. Whereas for our final conclusion, the results will be combined.

3.1 SSPG Experiment

In the SSPG experiment, all measurements were carried out at the same temperature of 300K. Nevertheless measurements were taken for both samples at different photon fluxes which was achieved by controlling the polarization of the laser beam. We estimated the luminous flux received by the photo detector at 633 nm with the formula:

$$F(cm^{-2}s^{-1}) = I(\mu A) \times 7.8 \cdot 10^{14} \tag{14}$$

For measuring the voltage of the photo diode, we finally computed the flux as:

$$F(cm^{-2}s^{-1}) = I(\mu A) \times 3.2 \cdot 10^{-4} \times 7.8 \cdot 10^{14} = V_{ph}(V) \times 2.5 \cdot 10^{11} \tag{15}$$

Figures 7 and 9 show the results of our SSPG beta fits (equation 3) for both samples A and B at both higher and lower flux and the corresponding linear, balberg fits (equation 4) are shown in figures 8 and 10 respectively.

The very good agreement between the two evaluation schemes of L_d and ϕ indicates the high quality of the measurements. We can also notice that fewer measurements were taken for sample A, this was because very small changes for the diffusion length were observed for a small increment in flux . So we needed some adequate change in the flux in order to observe an effect in the diffusion length.

Tables 2 and 3 together with figure 11 show the dependence of incident flux on the sample with the diffusion length for both samples A and B respectively. From this results we see an increase in the diffusion length with decreasing photon flux, which can be explained in two ways: (i) An increase in the flux impinging on the sample leads to an increase in the creation of more electron and holes which results in the shifting of the quasi Fermi levels towards the bands where the DoS is increasing due to the presence of the exponential tail states and thus creating more defect states which lower lifetime. (ii) another way we can interpret this is that an increase in flux might result in increasing absolute dangling bond density this leading to an increased recombination with the consequence of a reduction of the diffusion length.

Another observation from our experiment is a profound increase in the diffusion length for sample B (thicker sample) compared to sample A, this can be interpreted as that the quality of the material depends on the thickness, and it gets better and better with deposition time. Also we can say that the mean generation rate inside the thicker sample might be lower.

Photon flux $(cm^{-2}s^{-1})$	Diffusion length L_d (nm)
1.14×10^{17}	72.6
5.02×10^{16}	73.1
2.07×10^{16}	79.1
1.75×10^{16}	81.8

Table 2: Diffusion length at different fluxes for sample A

Photon flux ($cm^{-2}s^{-1}$)	Diffusion length L_d (nm)
1.24×10^{18}	88.35
1.13×10^{18}	97.16
9.97×10^{17}	102.09
8.80×10^{17}	106.12
6.10×10^{17}	109.38
4.75×10^{17}	111.22
3.12×10^{17}	112.52
1.25×10^{16}	117.55

Table 3: Diffusion length at different flux for sample B

(a) Highest

(b) Lowest
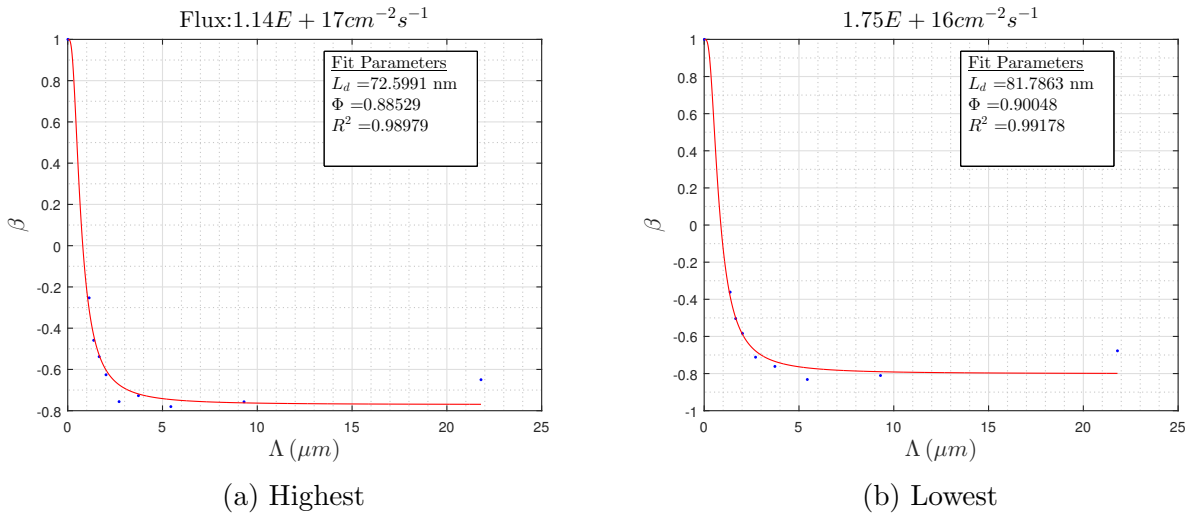
Fig. 7: Beta fit for sample A at different fluxes

(a) Highest

(b) Lowest
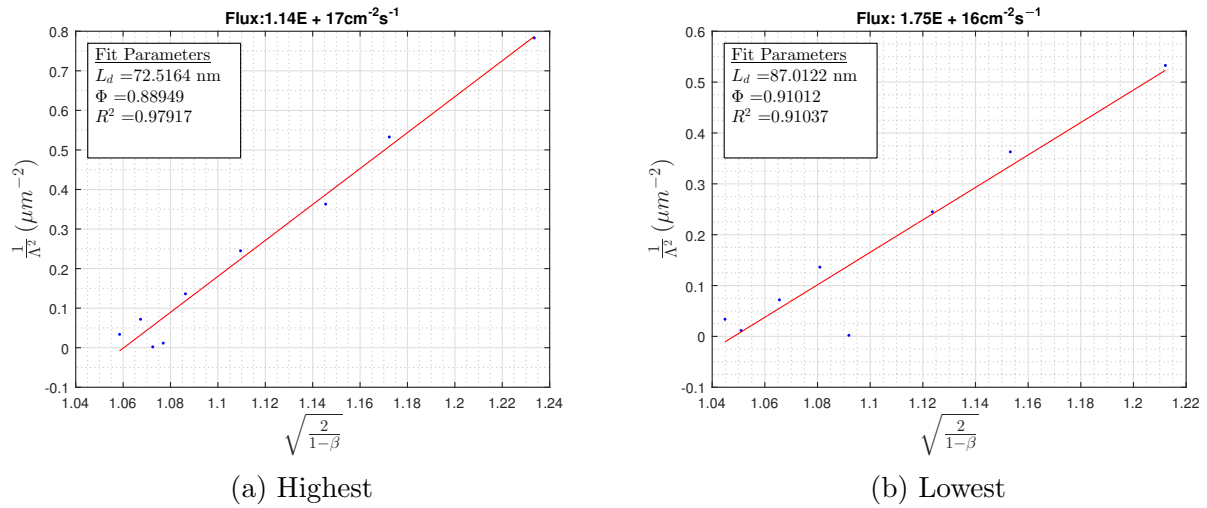
Fig. 8: Balberg fit for sample A at different fluxes

(a) Highest   (b) Lowest
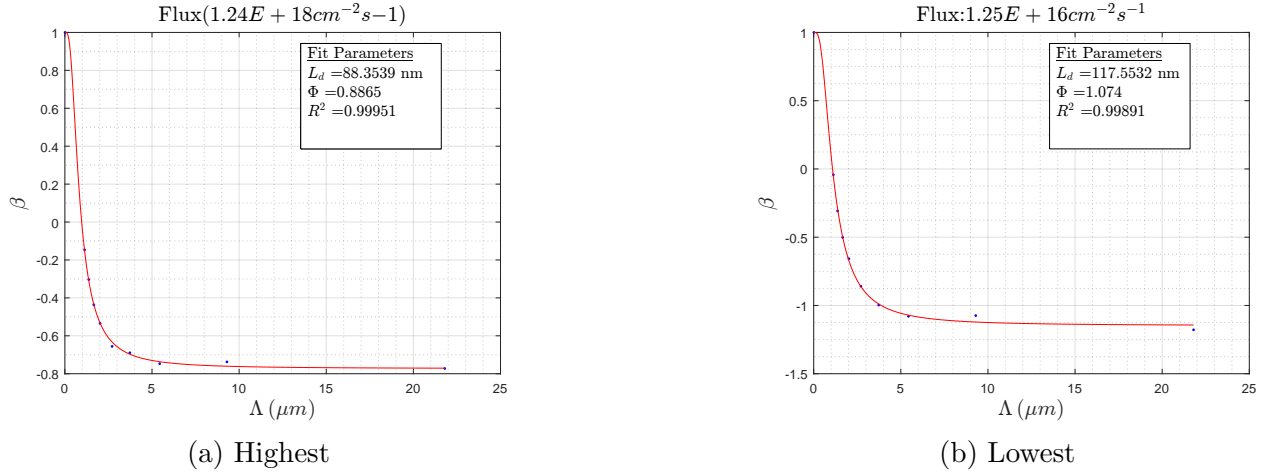
Fig. 9: Beta fit for sample B at different fluxes

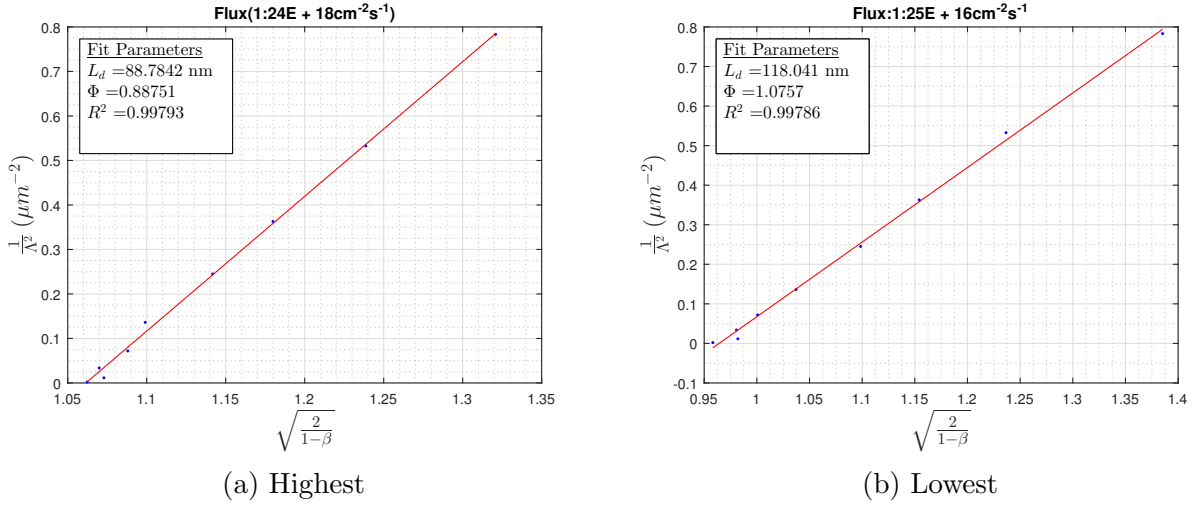

(a) Highest   (b) Lowest
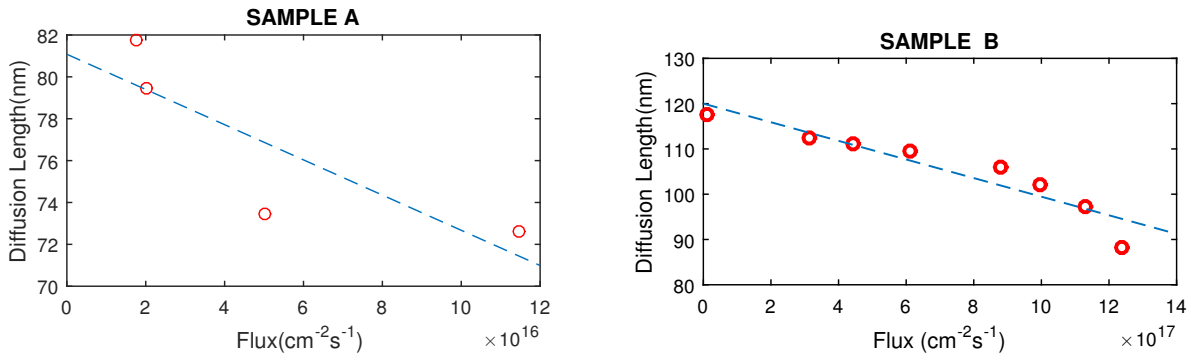
Fig. 10: Balberg fit for sample B at different fluxes

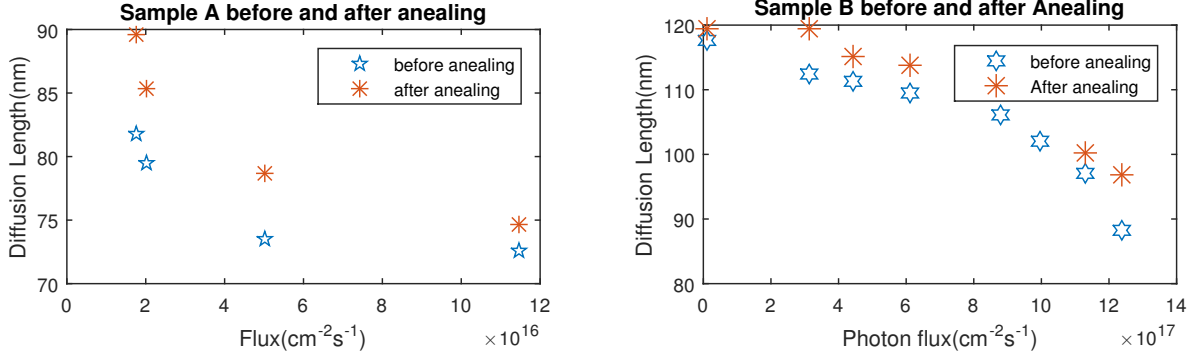Fig. 11: Diffusion length versus photon flux for sample A and sample B

Fig. 12: Diffusion length versus photon flux for sample A and B before and after annealing

3.2 Dark conductivity

Fig. 13 shows the photo-current in an Arrhenius plot measured with the setup depicted in Fig. 4 for different wavelengths and different illumination levels. The dark current flowing in the sample was measured for each value of λ and F_{dc}. These values should not change in principle, however small fluctuations were observed and therefore the mean, maximum and minimum value of the dark current are reproduced in the figure.

3.2.1 Observations for sample A

An almost linear decrease of the current under obscurity can be observed in the Arrhenius plot (exponential decay in linear space) for the high temperature region (430K - 300K). The measurements under light show a similar behavior for a very high temperature, but with a decreasing slope towards lower temperatures.

The highest photo-currents throughout the depicted region were observed for blue with an intensity of 1e15 cm^{-2}s^{-1} and the lowest ones for infrared with an intensity of 1e13 cm^{-2}s^{-1} . The photo-currents for the same color and for higher illumination levels are higher for all temperatures. For a constant intensity of 1e14 cm^{-2}s^{-1}, the photo-current increases from infrared over red to green, however it decreases again for blue.

3.2.2 Activation energy and dark Fermi level

The linear decrease of the dark current (in an Arrhenius plot) in the high temperature region corresponds to an activation energy. a-Si:H is even without doping slightly n-type in nature [3], and thus the carrier densities for electrons and holes above a few tens of Kelvin have the relationship of $n \gg p$. Furthermore the mobility of electrons is higher than the mobility of holes ($\mu_n \gg \mu_p$). Therefore the drift equation for the conductivity can be simplified:

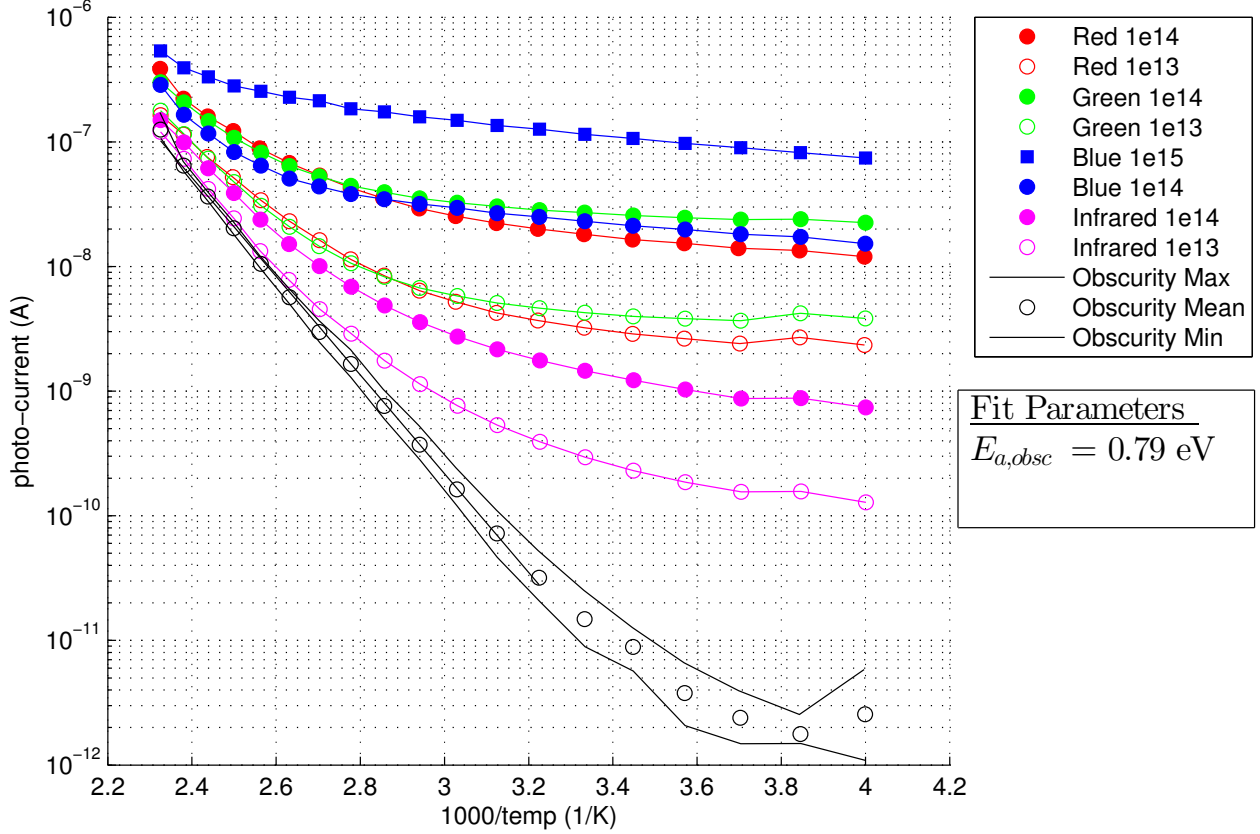$$\sigma = q(n\mu_n + p\mu_p) \approx qn\mu_n \quad \text{with} \quad n = N_c \exp \frac{-(E_c - E_F)}{kT}. \tag{16}$$

Fig. 13: Photo-current Arrhenius plot for sample A in the high temperature region (thickness d = 0.5 μm) under different illumination levels (cm⁻²s⁻¹).

Where σ is the conductivity, q the elementary charge, μ_n and μ_p the electron or hole mobility, n and p the electron or hole densities, N_c the effective density of states function in the conduction band, k the Boltzmann constant and $E_c - E_F$ the distance of the conduction band to the dark Fermi level.

The conductivity and the measured dark current are proportional to each other:

$$I = \sigma \frac{ht}{d} V_a \propto \sigma \tag{17}$$

Where I is the dark current, h, t and d the geometrical dimensions and V_a the applied voltage.

Therefore we can deduce the distance of the conduction band to the Fermi level in a-Si:H as slope in the Arrhenius plot:

$$\underbrace{\ln I}_{y} = \ln qn\mu_n \frac{ht}{d} V_a = \underbrace{-\frac{E_c - E_F}{k \cdot 1000}}_{m} \cdot \underbrace{\frac{1000}{T}}_{x} + \underbrace{\ln q\mu_n \frac{ht}{d} V_a N_c}_{b} \tag{18}$$

The value obtained for the sample A is 0.79 eV and for sample B 0.75 eV. Both energies match with the values described in literature to be in between 0.60 eV and 0.80 eV.
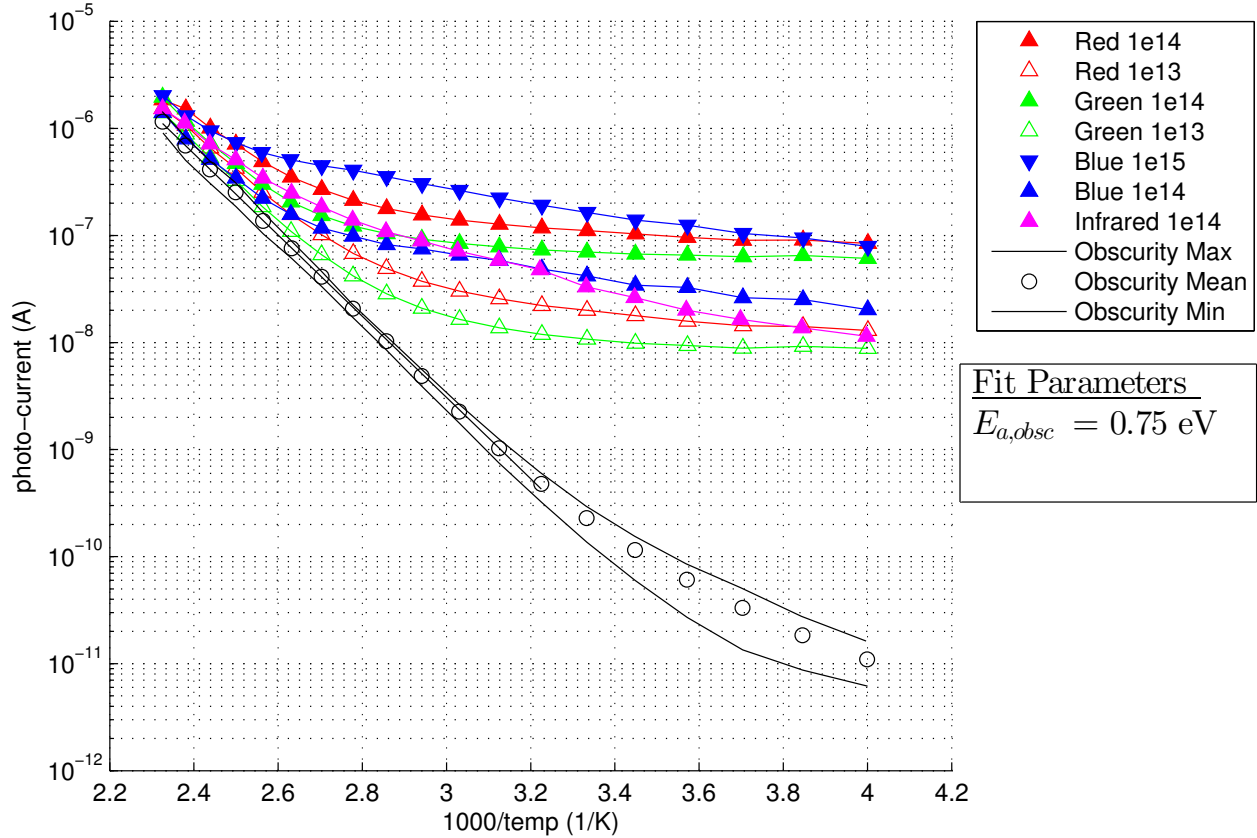
14

Fig. 14: Photo-current Arrhenius plot for sample B in the high temperature region (thickness d = 1.0 μm) under different illumination levels (cm^{-2}s^{-1}).

3.2.3 Explanations of observed behaviors

The similar slope for the photo-currents in comparison to the dark current for very high temperatures can be explained as for very high temperatures the carrier density through thermal excitation is so high that the excess generation through the incident light is negligible.

To observe the highest photo-current for blue with high intensity and the lowest photo-current for infrared (wavelength just above the bandgap) with low intensity is also an expected behavior, as the absorption increases with wavelength and a higher intensity leads to a higher electron and hole pair generation rate in the sample.

This explains also the differences observed for the same colors. A reason for the decrease in photo-current for blue could be that the recombination rate near the surface is higher due to surface recombination. As most of the blue light is absorbed near the surface because of the high absorption coefficient of a-Si:H for blue light, more carriers can recombine as for green light with a lower absorption coefficient.
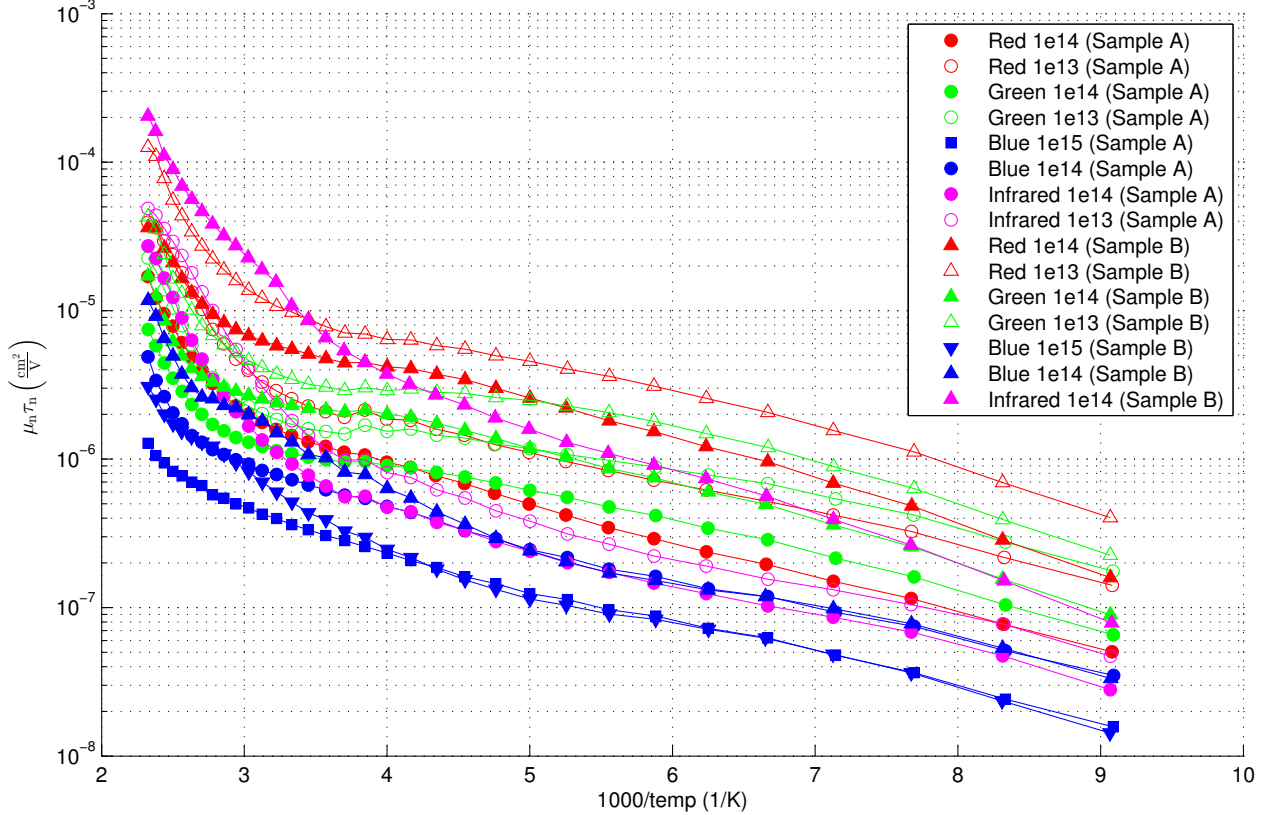
Fig. 15: Majority carrier mobility-lifetime product for a-Si:H.

3.2.4   Comparison to sample B

This observation is also supported by the measurements of sample B shown in Fig. 14. Here the highest photo-current for a photon flux of 1e14 cm^{-2}s^{-1} is observed for a longer wavelength as for sample A (for red instead of green as for sample A). Less carriers are lost near the surface (where the recombination rate is high) as they are more absorbed in the bulk of the thin film. As sample B is double as thick as sample A, it can absorb still a considerable amount of red carriers and less carriers are lost through non-absorption than through recombination in the case of green light.

3.3   Mobility lifetime product

Fig. 15 depicts the majority carrier mobility-lifetime product for sample A and sample B for different colors of incident light and different photon fluxes. The majority carrier mobility-lifetime product was calculated with equation 9. Table 4 shows the main parameters used for the measurements and the calculations.

3.3.1   Observations

A decrease of the mobility lifetime product $\mu_n \tau_n$ with decreasing temperature is observed. For the same color, $\mu_n \tau_n$ is higher if the flux of the incident light is lower. This seems to be related

16

Table 4: Used parameters for the SSPC and MPC measurements and calculations

Parameter	Value	Unit
$\lambda_{infrared}$	720	nm
λ_{red}	625	nm
λ_{green}	525	nm
λ_{blue}	450	nm
$\alpha_{infrared}$	1e3	cm^{-1}
α_{red}	1e4	cm^{-1}
α_{green}	3e4	cm^{-1}
α_{blue}	1e5	cm^{-1}
μ_n	10	cm^{2}V^{-1}s^{-1}
V_a	100	V
R	0	
η	1	

to the increase of the diffusion length for lower light intensities which was observed for SSPG in section 3.1.

Fig. 16 and Fig. 17 show $\mu_n\tau_n$ for only one flux of 1e13 cm^{-2}s^{-1} or 1e14 cm^{-2}s^{-1} respectively, for both only in the high temperature region. At 300 K, $\mu_n\tau_n$ is highest for red for sample A and B, except for sample B for a flux of 1e14 cm^{-2}s^{-1} where infrared is performing best. The differences of $\mu_n\tau_n$ between sample A and sample B decrease with increasing photon energy and in the case of blue (for 1e14 cm^{-2}s^{-1}), the difference which can be observed is very low. The values for $\mu_n\tau_n$ of sample B are generally higher than those of sample A. The margin is highest for infrared light and decreases with increasing photon energy and is almost zero for blue light.

With increasing temperature, the majority carrier mobility-lifetime product increases.

3.3.2   Explanation of the observed behavior

This could be due to an increase of the majority carrier mobility μ_n because of a higher kinetic energy of the carriers, if the carrier lifetime τ_n is assumed to be constant with temperature.

A higher $\mu_n\tau_n$ for a lower photon intensity can be explained as that the Quasi Fermi levels (QFs) interact with the exponential tail states (which can be measured through MPC) when the QFs approach the conduction and valence band. This leads to an exponential increase of the occupied defect states which promotes recombination.

Also a link to the SSPG experiment can be made as the diffusion length L_d is related with the minority carrier lifetime τ_p through the diffusivity D:

$$L_d = \sqrt{D\tau_p} \tag{19}$$
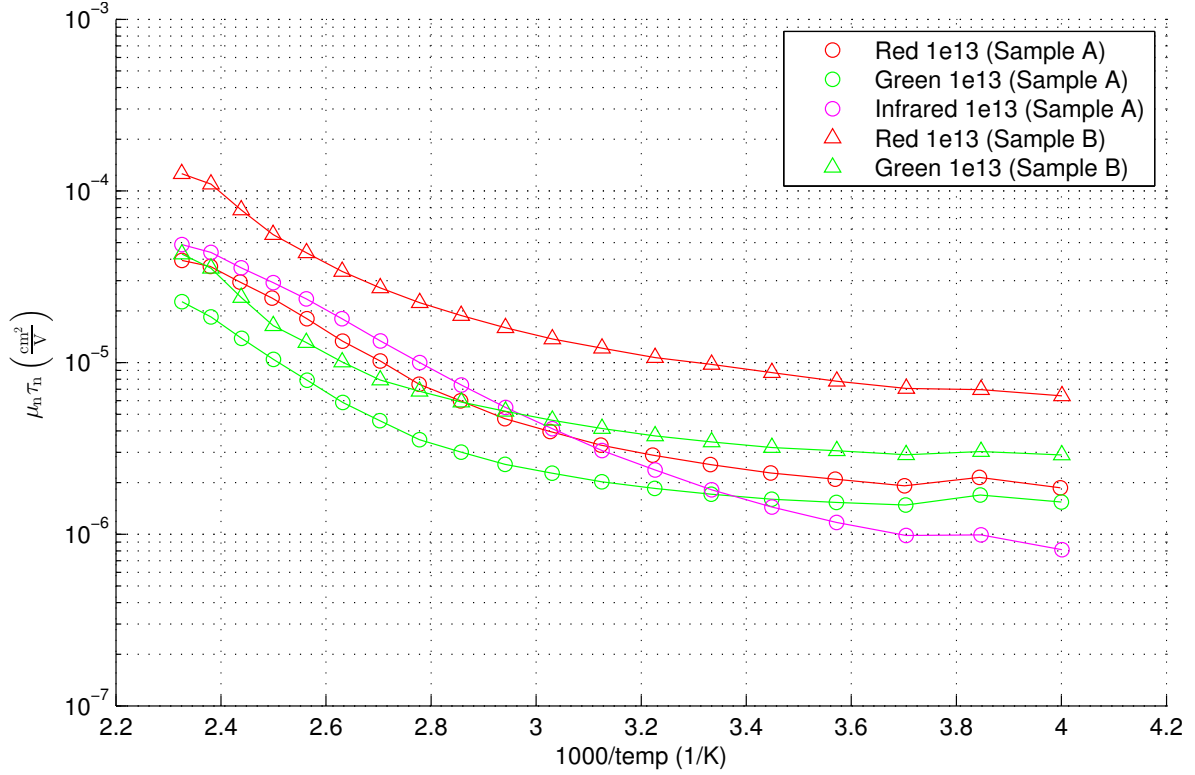
Fig. 16: Majority carrier mobility-lifetime product for a photon flux of 1e13 cm^{-2}s^{-1} .
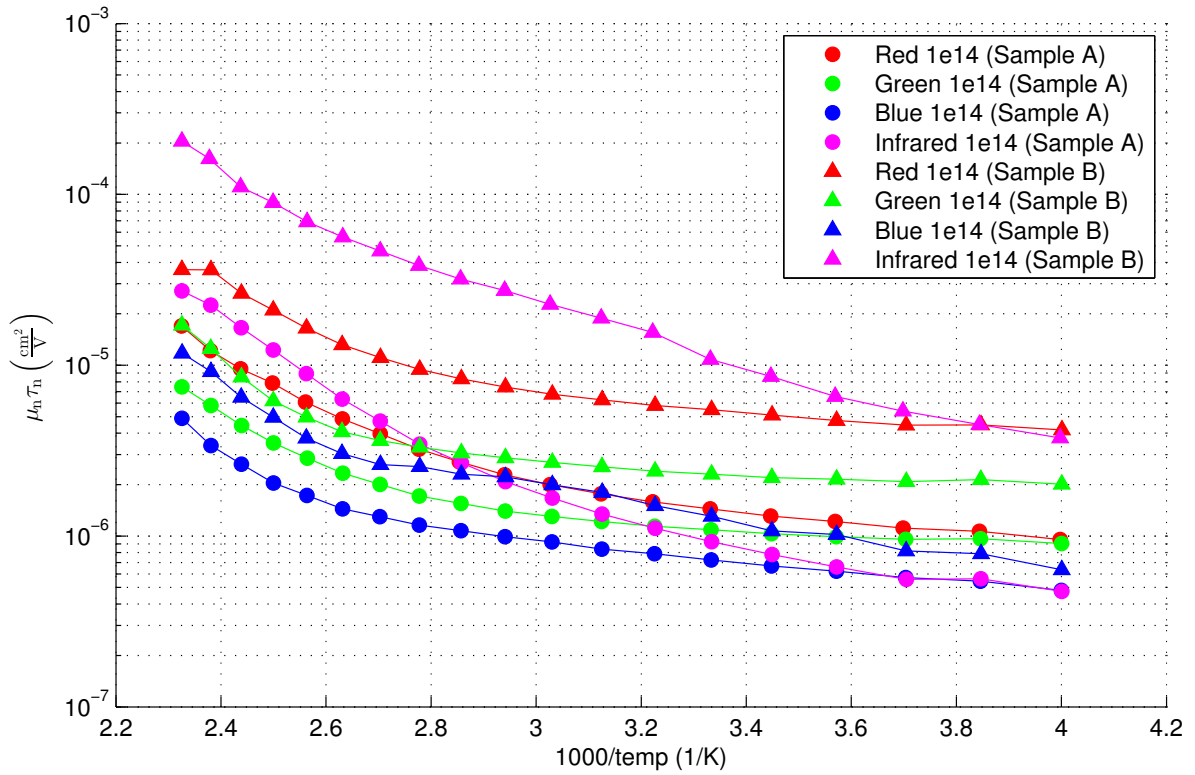

Fig. 17: Majority carrier mobility-lifetime product for a photon flux of 1e14 cm^{-2}s^{-1} .

Table 5: Mobility lifetime products and lifetimes for different samples at 300K, lifetime calculated for quantum efficiency $\eta = 1$ and mobility $\mu_{\mathrm{n}} = 10\frac{\mathrm{cm}^2}{\mathrm{Vs}}$

Sample	$\mu_{\mathbf{n}}\tau_{\mathbf{n}}\left(\frac{\mathbf{cm^2}}{\mathbf{V}}\right)$	$\tau_{\mathbf{n}}\ (\boldsymbol{\mu}\mathbf{s})$
Red 1e14 (Sample A)	1.44e-06	0.14
Red 1e13 (Sample A)	2.55e-06	0.25
Green 1e14 (Sample A)	1.09e-06	0.11
Green 1e13 (Sample A)	1.71e-06	0.17
Blue 1e15 (Sample A)	3.62e-07	0.04
Blue 1e14 (Sample A)	7.25e-07	0.07
Infrared 1e14 (Sample A)	9.26e-07	0.09
Infrared 1e13 (Sample A)	1.82e-06	0.18
Red 1e14 (Sample B)	5.49e-06	0.55
Red 1e13 (Sample B)	9.77e-06	0.98
Green 1e14 (Sample B)	2.30e-06	0.23
Green 1e13 (Sample B)	3.45e-06	0.34
Blue 1e15 (Sample B)	5.12e-07	0.05
Blue 1e14 (Sample B)	1.31e-06	0.13
Infrared 1e14 (Sample B)	1.08e-05	1.08

Furthermore we can make the assumption that the minority carrier lifetime τ_p is related to the majority carrier lifetime τ_n. In the SSPG experiments, it was observed that L_d increased with decreasing light intensity. If L_d increases, also the lifetime of the minority carriers τ_p increases. This leads to the same conclusion as above, that $\mu_n\tau_n$ increases with decreasing photon flux.

The fact that the difference between $\mu_n\tau_n$ for sample A and B increases with increasing wavelength can be understood if we consider that most of the blue light is absorbed near the surface (penetration depth of 0.1 μm for $\alpha_{blue} = 1e5\ cm^{-1}$) and thus the thickness of the material is much higher (> 0.5 μm). This holds less and less true for decreasing wavelengths up to infrared. That for sample B higher values for $\mu_n\tau_n$ are observed for large wavelengths can be explained through superior bulk conduction parameters. Thus the mobility lifetime product in the bulk is higher in sample B than in sample A.

Table 5 lists the majority carrier mobility-lifetime products and lifetimes for the two samples under different conditions (light intensity and wavelength) at 300 K. The values of $\mu_n\tau_n$ reported here are among the highest values reported in literature for this material (cp. [3], for electrons between 5e-6 and 5e-8 cm^2V^{-1}). The highest value was observed for sample B with infrared color and 1e14 $cm^{-2}s^{-1}$ light intensity with 1.08e-5 cm^2V^{-1}. The lowest value accordingly for sample A with blue light and an intensity of 1e15 $cm^{-2}s^{-1}$ at 3.62e-7 cm^2V^{-1}.

3.4 MPC Experiment

3.4.1 Objective

As previously explained we are studying two hydrogenated amorphous silicon samples (a-Si:H), deposited on glass through PECVD[1], one with a thickness of 0.5 μm (sample 1) and the other with 1.0 μm (sample 2).

The objective of the MPC measurements is the do a reconstruction of the localized density of states (r-DoS from now on).

We want to study how the technique works, and to study the effect of: Photon flux, absorption coefficient (wavelength), thickness of the sample and capture coefficient. Indeed, in a recent work from GeePs laboratory, 2D simulations of the MPC experiment have predicted a strong effect of the photogeneration inhomogeneity in the sample on the reconstruction of the DoS, that could lead to misinterpretations [5].

3.4.2 Parameters

The r-DoS depend on several parameters which have to be estimated. In table 6 are shown the values used for the electrical parameters, which are typical values.

Parameter	Notation	Unit	Value
Electron Mobility	μ_n	$cm^3 s^{-1}$	10
Conduction band DoS	N_C	cm^{-3}	1×10^{19}
Electron Capture Coefficient[2]	c_n	$cm^2 V^{-1} s^{-1}$	1×10^{-8}

Table 6: Main electrical parameters used

The absorption coefficient (α) is also an important parameter and depends on the wavelength. The absorption coefficient will have an influence on the light penetration depth and, in turn, on the current cross section (see figure 1b). The following values were used:

Color	Wavelength (nm)	α (cm^{-2})
Infrared	740	1×10^3
Red	625	1×10^4
Green	525	3×10^4
Blue	450	1×10^5

Table 7: Absorption coefficient

As for the light fluxes, a value for the DC and AC Fluxes was set. In order to obtain lower fluxes, an optical filter with an attenuation of 10 was used. The following values were set:

---

[1]Plasma-enhanced chemical vapor deposition

[2]The value of the capture coefficient is the most difficult to estimate, thus in the data treatment this parameter was changed in order to understand its influence

- **Without attenuation:** DC flux $= 1 \times 10^{14}\ cm^{-2}s^{-1}$, AC flux $= 3 \times 10^{13}\ cm^{-2}s^{-1}$

- **With attenuation:** DC flux $= 1 \times 10^{13}\ cm^{-2}s^{-1}$, AC flux $= 3 \times 10^{12}\ cm^{-2}s^{-1}$

Except for the blue light, for which the fluxes where 10 times higher.
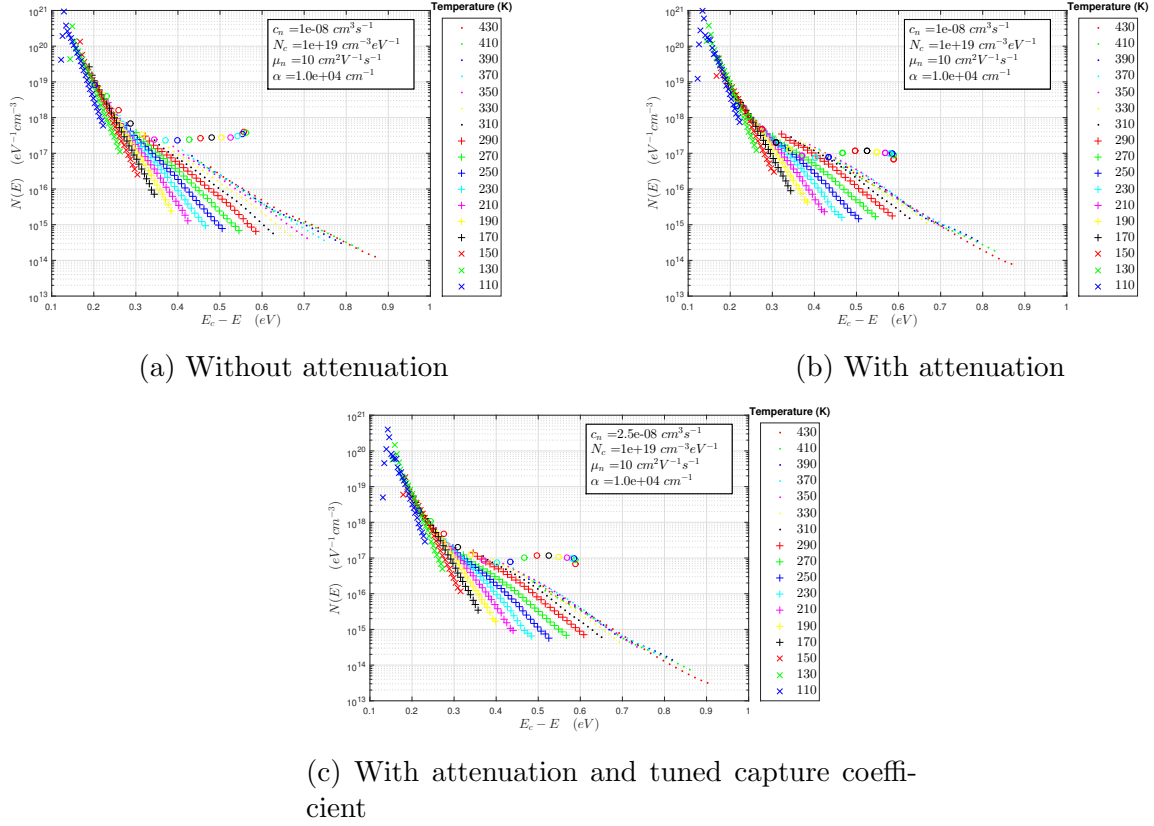
3.4.3 Results

Sample A

(a) Without attenuation

(b) With attenuation

(c) With attenuation and tuned capture coefficient

Fig. 18: *Sample A* MPC r-DoS under **red** light illumination; HF in dots and crosses, LF in circles
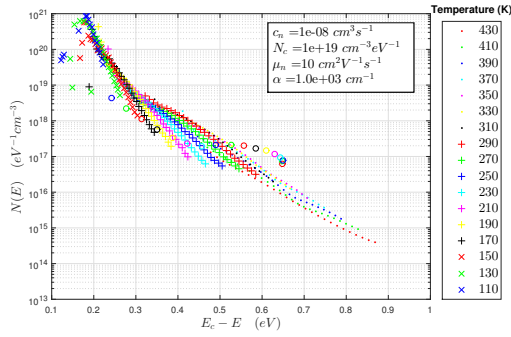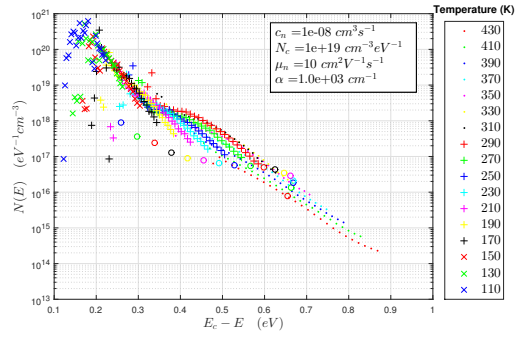

(a) Without attenuation
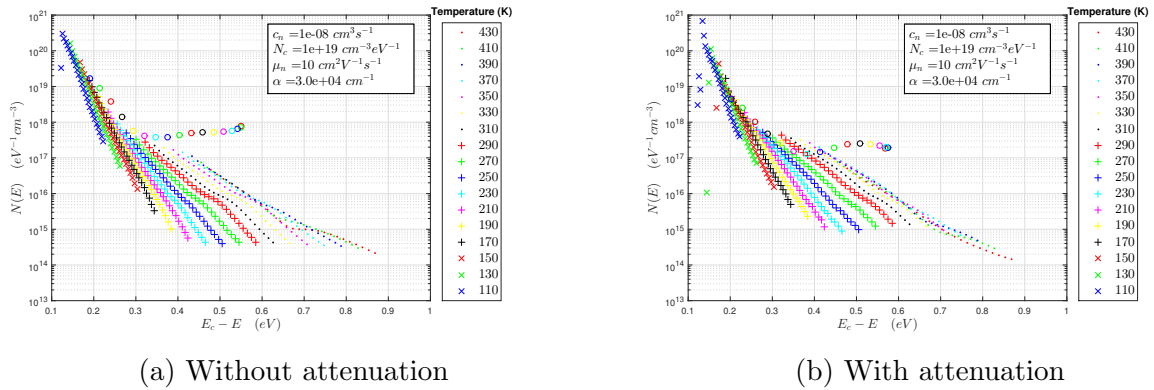
(b) With attenuation

Fig. 19: *Sample A* MPC r-DoS under **green** light illumination; HF in dots and crosses, LF in circles
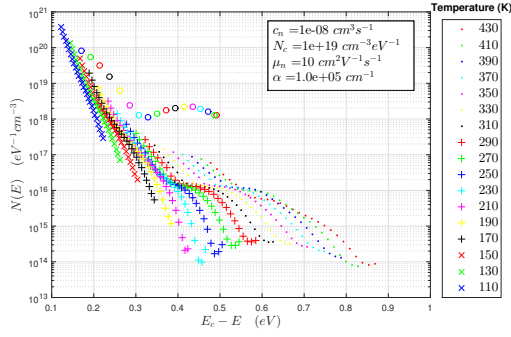
(a) Without attenuation
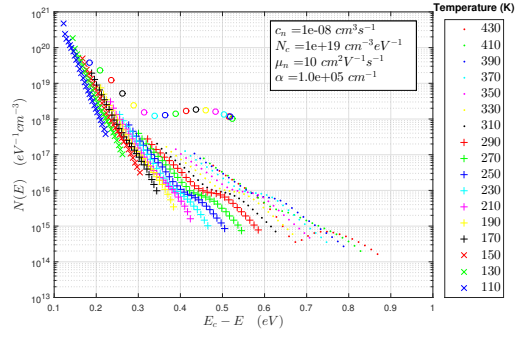
(b) With attenuation

Fig. 20: *Sample A* MPC r-DoS under **blue** light illumination; HF in dots and crosses, LF in circles
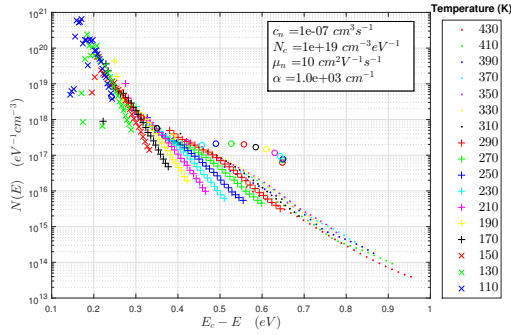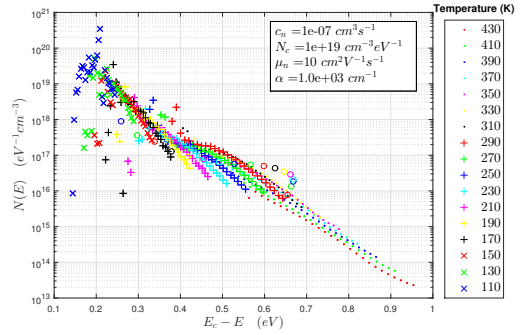
Sample B

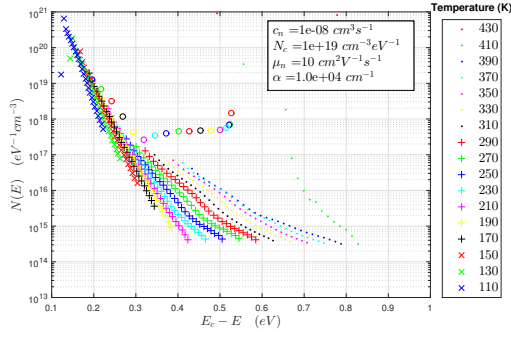(a) Without attenuation

(b) With attenuation

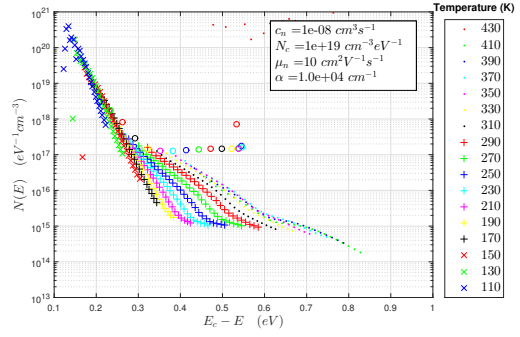(c) Without attenuation and tuned capture coefficient

(d) With attenuation and tuned capture coefficient

Fig. 21: *Sample B* MPC r-DoS under **infrared** light illumination; HF in dots and crosses, LF in circles
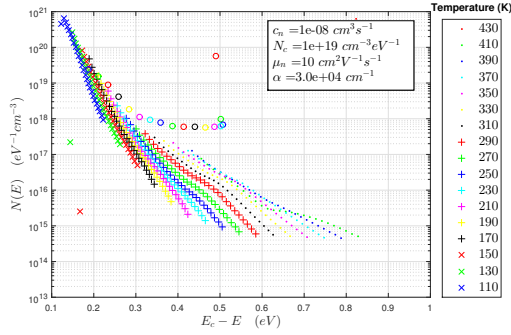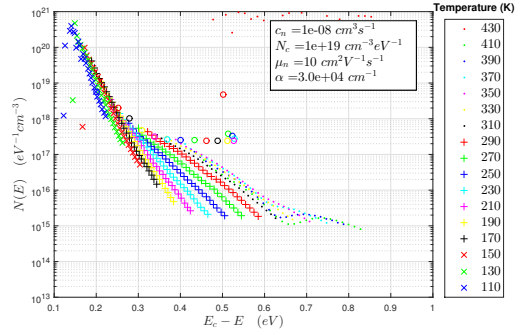
(a) Without attenuation

(b) With attenuation

Fig. 22: *Sample B* MPC r-DoS under **red** light illumination; HF in dots and crosses, LF in circles
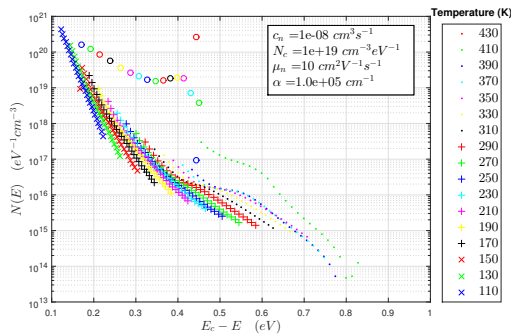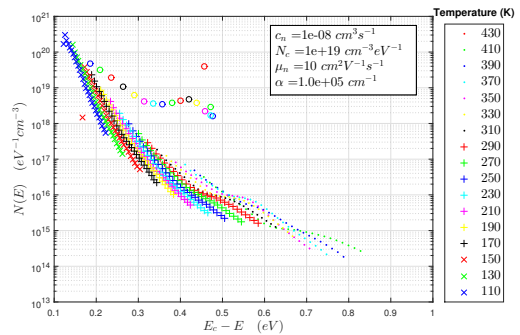

(a) Without attenuation

(b) With attenuation

Fig. 23: *Sample B* MPC r-DoS under **green** light illumination; HF in dots and crosses, LF in circles

(a) Without attenuation

(b) With attenuation

Fig. 24: *Sample B* MPC r-DoS under **blue** light illumination; HF in dots and crosses, LF in circles

3.4.4 Description of the Figures

In the plots below, we can distinguish the temperatures by color. The higher temperatures allow the electrons to be captured (and re-emitted) by states closer to the middle of the band gap while lower temperatures allow electrons to only interact with the states closer to the conduction band. We can also distinguish the two regimes by the form of the data points (dots and crosses for the HF and circles for the LF). The expected behavior for this two series of data is that their values are close until a certain energy level (closer to the center of the band gap) where they start to diverge. Before this divergence the r-DoS is more accurately obtained by the upper envelope of the data, namely the HF data, which models the tail states. Once they start to diverge the LF data starts to be more accurate in modeling the deep-states, than the HF regime.

For the HF regime all frequencies where plotted, although only the highest values are relevant to generate the r-DoS. Contrarily, for the LF regime only the lowest frequency was used, which should be the most accurate one. Nevertheless, in order to choose the right frequencies for the LF regime, the logarithmic plot of $\tan(\phi)$ vs frequency should be analyzed in order to verify the validity of the LF regime, which is, as we have seen before in figure 6, never completely valid.

We can see in figures 22, 23 and 24, that in these cases the high temperature values do not have any meaning. This is more likely due to a too high gain in the look-in amplifier, saturating it.

3.4.5 MPC discussion

As explained before the parameters chosen might not be the most accurate ones. One of the parameters which seems to be more likely to change is the capture coefficient. It is known that the value of the capture coefficient can be different between tail states (HF) and deep states (LF).

As we can see in all plots, when the light is attenuated the LF DoS is below the DoS of the HF regime. The most likely reason for this is due to the filter used, which might not have the expected attenuation factor, or that the capture coefficient chosen is not accurate enough. Two parameters where changed to try to verify this. First the light fluxes where changed to a lower attenuation factor, but this resulted in the same plot but with lower values for r-DoS. By changing the capture coefficient to $2.5 \times 10^{-8} \ cm^{-3}s^{-1}$ in figure 18 c) it was possible to obtain a reasonable plot of the DoS, but also with lower than expected r-DoS in comparison with the non attenuated, although there is no obvious reason for the c_n to be dependent on light flux.

In order to better understand what is the reason behind this, it would be useful to get a more accurate value of the capture coefficient and redo the figures. It would be also advisable to measure the attenuation factor of the filter using a power meter.

Another case where tuning the capture coefficient seems necessary is with the infrared light shown in figure 21. As we can see, the LF DoS are always bellow the HF DoS. This might be due to the low energy of the irradiation (just above the band gap), meaning that the exited electrons end up having very little kinetic energy, thus having a higher recombination rate. As a result, if the capture coefficient is maintained, the HF DoS will have a higher value than expected due to a lower output current. This is why in this case choosing an capture coefficient of $1 \times 10^{-7} \ cm^{-3}s^{-1}$ gives more reasonable results. In the LF DoS reconstruction, there is also an energy shift to higher

values, confirming the previous hypothesis.

Another reason might be related with the estimation of the current flow cross section, as shown in figure 1. Although the absorption coefficient was taken into account to obtain the cross section, is was assumed that it is the vertical area from the surface until the effective range of the photon flux. This can give rise to errors mainly for low absorption coefficients, because the electrons are generated in the lower part of the samples and thus the current flux might not travel through the same cross section as the ones generated on the upper part.

Another observable phenomena is an offset between the LF r-DoS and the HF r-DoS for low wavelength values of the radiation. This has to do with limitations of the 1D approximation used to compute the equations for the MPC experiment explained by R. Lachaume et al. [5]. The phase shift overshoot happens because states deep in the sample (far from the surface) are still in HF. there is also the effect of the diffusion of photo carriers at the surface towards the bulk, which decreases the concentration at the surface. these effects are 2D and are not taken into account in the 1D formulas.

Another effect of higher energy photons is a displacement in energy for the LF DoS reconstruction, this might be due to the presence of holes which is neglected in the formula.

4   Conclusion

In the SSPG experiments, the very good agreement between the two evaluation schemes for L_d indicates the high quality of the measurements. It should be mentioned that it is not possible to achieve such a good agreement for all samples under all the different conditions like for lowest or highest flux. Any deviations between the values of the two analyses can be investigated and in some cases removing individual data points may results in better results. The experimental error in the linear plot may become bigger for a larger β because of the $(1 - \beta)$ term in the denominator in equation 4.

Also the results from both samples indicate an improvement in the sample performance through annealing. This is shown as an increase in the diffusion length after the samples were annealed.

In the SSPC measurements, a value for the distance between the conduction band and the Fermi level $E_c - E_F$ has been found, which matches with the literature for both samples (of different thicknesses). In addition, the photo-current increased for higher light intensies and was highest for green light for sample A (0.5 µm thickness) and for red light for sample B (1.0 µm thickness).

The mobility lifetime product increased with higher temperatures and the biggest values at 300 K were observed for red light shined on sample A and for red or infrared light shined on sample B (depending on light flux). The mobility lifetime product increased with decreasing light intensity (e.g. for sample B with red light from 5.49e-6 to 9.77e-6 cm^{2}V^{-1} for a decrease of light intensity by 10 from 1e14 to 1e13 cm^{-2}s^{-1}). As the mobility lifetime product for blue with the same intensity was very similar for both samples, it can be concluded that the front surface has similar conduction properties for both samples. However the bulk conduction properties of sample B are superior to the ones of sample A. The highest value of $\mu_n \tau_n$ observed was higher than the range reported in the literature, which suggests that the material of both samples is very good in terms of transport properties in comparison to already existing materials.

We can say that the MPC reconstruction of the DoS for a-Si:H was in accordance with the predicted results form theoretical models. The biggest difficulty in obtaining an accurate r-DoS lies in the estimation of the unknown parameters. Although common values for a-Si:H were used, these parameters change depending on the deposition process and, possibly thickness, consequently it is hard to have accurate values.

It seems that the thinner sample shows a more precise LF r-DoS than the thicker one. This is again an argument that the expression used to obtain the current cross section has to be analyzed.

Changing the color modifies the photo generation profile in the sample and also the response of the samples to the modulated light. The red light gives the most accurate results since the absorption is quite homogeneous. This case is more likely to be suitable for applying the 1D reconstruction formulas.

It seems that for blue light, the strong gradient of photo generation leads to an overestimation of the LF DoS. This phenomenon is explained by the recent work of GeePs. These measurements are good illustrations for their 2D simulations.

It would be interesting to do 2D simulations and try to fit the experimental results, and then to compare them with the current model.

It seems important to use both LF and HF reconstructions to guarantee the accuracy of the reconstruction. Though the HF reconstruction seems to be more independent of the 2D effects.

The mobility lifetime product increases with a decrease of photon flux which is related to the increase of the diffusion length observed in the SSPG experiment as well as to the exponential band tail measured in the HF-MPC experiment.

The surface transport properties near the surface seem to be comparable for both samples according to the SSPC measurements. The SSPG experiment however clearly shows that the sample B is superior to sample A because it has a higher minority carrier diffusion length L_d, especially for lower light intensities (81.8 nm for sample A and 117.5 nm for sample B).

The laboratory was very useful for us in terms of data analysis and the handling of scientific analysis equipment and software, such as the SSPG and SSPC/MPC setup at GeePs and their control with LabView or the analysis of the data with Matlab.

Acknowledgments

References

[1] Amir Fath Allah. *Regroupement de techniques de caractérisation de matériaux destinés à l'énergie solaire pour optimisation et mesures industrielles.* PhD thesis, Université Paris Sud, 7 2015. 5

[2] R Brüggemann. Steady-state photocarrier grating technique for the minority-carrier characterisation of thin-film semiconductors. *Journal of Physics: Conference Series*, 253(1):012081, 2010. 3

[3] A FathAllah, F Ventosinos, and C Longeaud. An automated experiment for determination of thin film semiconductor transport parameters. *Journal of Physics: Conference Series*, 558(1):012011, 2014. 9, 13, 19

[4] GeePs. *Notice Technique; Appareil SSPG automatique; Description, mise en route et réglages.* 11, rue Joliot Curie Plateau de Moulon 91192 Gif sur Yvette Cedex, 2014. 5

[5] Raphaël Lachaume, Christophe Longeaud, and Jean-Paul Kleider. New insights into the modulated photocurrent technique using 2D full numerical simulations. In *26th International Conference on Amorphous and nanocrystalline Semiconductors (ICANS 26)*, Aachen, Germany, September 2015. 20, 26

[6] D. Ritter, E. Zeldov, and K. Weiser. Steady-state photocarrier grating technique for diffusion length measurement in photoconductive insulators. *Applied Physics Letters*, 49(13):791–793, 1986. 4